Unraveling the time cross correlations of an emitter switching between two states with the same fluorescence intensity

F Eloi, H Frederich, A Leray, S Buil, Xavier Quélin, B Ji, Emerson Giovanelli, N Lequeux, B Dubertret, J.-P Hermier

Unraveling the time cross correlations of an emitter switching between two states with the same fluorescence intensity

F. Eloi[1], H. Frederich[1], A. Leray[2], S. Buil[1], X. Quélin[1], B. Ji[3], E. Giovanelli[3], N. Lequeux[3], B. Dubertret[3], and J.-P. Hermier[1,4,⋆]

[1] *Groupe d'Etude de la Matière Condensée (GEMaC), Université de Versailles-Saint Quentin en Yvelines, CNRS UMR 8635, Université Paris-Saclay, 45 avenue des Etats-Unis, 78035 Versailles Cedex, France*

[2]*Laboratoire Interdisciplinaire Carnot de Bourgogne (ICB), UMR 6303 CNRS, Université de Bourgogne, 9 Avenue Savary, BP 47870, 21078 Dijon Cedex, France*

[3]*Laboratoire de Physique et d'Étude des Matériaux, CNRS UMR8213, ESPCI, 10 rue Vauquelin, 75231 Paris, France*

[4]*Institut Universitaire de France, 103, Bd Saint-Michel, 75005 Paris, France*

⋆*jean-pierre.hermier@uvsq.fr*

Abstract: The autocorrelation function of the fluorescence intensity of a nanoemitter is measured with the standard Hanbury-Brown and Twiss setup. Time-tagging of the photodetection events during all the experiment has opened new possibilities in terms of post-selection techniques that enable to go beyond the blinking and antibunching characterization. Here, we first present a new method developed to investigate in detail the antibunching of a fluorophore switching between two emitting states. Even if they exhibit the same fluorescence intensity, their respective amount of antibunching can be measured using the gap between their respective decay rates. The method is then applied to a nanoemitter consisting in a colloidal quantum dot coupled to a plasmonic resonator. The relative quantum efficiency of the charged and neutral biexcitons are determined.

OCIS codes: (270.5290) Photon statistics; (300.6500) Spectroscopy, time-resolved; (230.5590) Quantum-well, -wire and -dot devices; (250.5403) Plasmonics.

References and links

1. P. Grangier, G. Roger, and A. Aspect, "Experimental Evidence for a Photon Anticorrelation Effect on a Beam Splitter: A New Light on Single Photon Interferences," Europhys. Lett. **1**, 173-179 (1986).
2. T. Basché, W. E. Moerner, M. Orrit, and H. Talon, "Photon antibunching in the fluorescence of a single dye molecule trapped in a solid," Phys. Rev. Lett. **69**, 1516-519 (1992).
3. R. Brouri, A. Beveratos, J.-P. Poizat, and P. Grangier, "Photon antibunching in the fluorescence of individual color centers in diamond," Opt. Lett. **25**, 1294-1296 (2000).
4. P. Michler, A. Kiraz, C. Becher, W. V. Schoenfeld, P. M. Petroff, L. Zhang, E. Hu, and A. Imamoglu, "A quantum dot single-photon turnstile device," Science **290**, 2282-2285 (2000).
5. P. Michler, A. Imamoglu, M. D. Mason, P. J. Carson, G. F. Strouse, and S. K. Buratto, "Quantum correlation among photons from a single quantum dot at room temperature," Nature **406**, 968-970 (2000).
6. G. Nair, J. Zhao, and M. G. Bawendi, "Biexciton Quantum Yield of Single Semiconductor Nanocrystals from Photon Statistics," NanoLetters. **11**, 1136-1140 (2011).

7. D. Canneson, L. Biadala, S. Buil, X. Quélin, C. Javaux, B. Dubertret, and J.-P. Hermier, "Blinking suppression and biexcitonic emission in thick-shell CdSe/CdS nanocrystals at cryogenic temperature," Phys. Rev. B **89**, 035303 (2014).
8. B.D. Mangum, Y. Ghosh, J. A. Hollingsworth, and H. Htoon, "Disentangling the effects of clustering and multi-exciton emission in second-order photon correlation experiments," Opt. Expr. **21**, 7419-7426 (2013).
9. W. B. Gao, P. Fallahi, E. Togan, J. Miguel-Sanchez, and A. Imamoglu, "Observation of entanglement between a quantum dot spin and a single photon. Nature **49**, 426-430 (2012).
10. K. De Greve, L. Yu, P. L. McMahon, J. S. Pelc, C. M. Natarajan, N. Y. Kim, E. Abe, S. Maier, C. Schneider, M. Kamp, S. Hofling, R. H. Hadfield, A. Forchel, M. M. Fejer, Y. Yamamoto, "Quantum-dot spin-photon entanglement via frequency downconversion to telecom wavelength," Nature **491**, 421-425 (2012).
11. J. R. Schaibley, A. P. Burgers, G. A. McCracken, L.-M. Duan, P. R. Berman, D. G. Steel, A. S. Bracker, D. Gammon, and L. J. Sham. "Demonstration of quantum entanglement between a single electron spin confined to an InAs quantum dot and a photon," Physical review letters **110**, 167401 (2013).
12. P. Spinicelli, S. Buil, X. Quélin, B. Mahler, B. Dubertret and J.-P. Hermier, "Bright and Grey States in CdSe-CdS Nanocrystals Exhibiting Strongly Reduced Blinking," Phys. Rev. Lett **102**, 136801 (2009).
13. Al. L. Efros and M. Rosen, "Random Telegraph Signal in the Photoluminescence Intensity of a Single Quantum Dot," Phys. Rev. Lett. **78**, 1110 (1997).
14. K. Matsuda, Y. Ito, and Y. Kanemitsu, Appl. Phys. Lett. **92**, 211911 (2008)
15. Y. Wang, T Yang, M. T. Tuominen, and M. Achermann, "Radiative Rate Enhancements in Ensembles of Hybrid Metal-Semiconductor Nanostructures," Phys. Rev. Lett. **102**, 163001 (2009).
16. Y. Ito, K. Matsuda, and Y. Kanemitsu, "Mechanism of photoluminescence enhancement in single semiconductor nanocrystals on metal surfaces," Phys. Rev. B **75**, 033309 (2007).
17. T. J. Lin, W. J. Chuang, S. Cheng, and Y. F. Chen, "Enhancement of emission from CdSe quantum dots induced by propagating surface plasmon polaritons," Appl. Phys. Lett. **94**, 173506 (2009).
18. I. Mallek-Zouari, S. Buil, X. Quélin, B. Mahler, B. Dubertret, and J.-P. Hermier, "Plasmon assisted single photon emission of CdSe/CdS nanocrystals deposited on random gold film," Appl. Phys. Lett. **97**, 053109 (2010).
19. B. Ji, E. Giovanelli, B. Habert, P. Spinicelli, M. Nasilowski, X. Xu, N. Lequeux, J.-P. Hugonin, F. Marquier, J-J. Greffet and B. Dubertret, "Non-blinking quantum dot with a plasmonic nanoshell resonator," Nat. Nanotech. **10**, 170-175 (2015).
20. F. García-Santamaría, Y. Chen, J. Vela, R. D. Schaller, J. A. Hollingsworth, and V. I. Klimov, "Suppressed Auger Recombination in "Giant" Nanocrystals Boosts Optical Gain Performance," NanoLett. **9**, 3482 (2009).
21. A. Leray, C. Spriet, D. Trinel, Y. Usson Y, and L. HÃ©liot, "Generalization of the polar representation in time domain fluorescence lifetime imaging microscopy for biological applications: practical implementation," J. Microsc. **248**, 66-76 (2012).
22. B. E. Brinson, J. B. Lassiter, C. S., R. Bardhan, N. Mirin, and N. J. Halas, "Nanoshells made easy: improving Au layer growth on nanoparticle surfaces," Langmuir **24**, 14166-14171 (2008).

1. Introduction

Single photon sources such as atoms [1], molecules [2], NV centers in diamond [3], molecular beam epitaxial [4] and colloidal quantum dots [5] have been extensively studied using the autocorrelation function (ACF) of the intensity $g^{(2)}(\tau)$. Through the ACF measured with the Hanbury-Brown and Twiss (HBT) setup, non classical light properties can be characterized and the antibunching effect synonymous of a light beam with sub-poissonian statistics can be demonstrated. Beyond the proof of single photon emission, cross correlation experiments can also provide either the radiative quantum efficiency (QE) of the biexcitonic recombination in semiconductor quantum dots [6] or a full characterization of the flickering over time scales ranging from few nanoseconds to seconds [7].

Progresses in the conception and realization of electronic devices have enabled to reduce dramatically the size of the electronic setups that record the photodetection events. The time resolution has also been improved and reaches sub-ps values. More fundamentally, the most recent devices enable to time-tag the absolute arrival time of the detected photons with a time accuracy of the order of 100 ps during all the duration of the experiment. From a single set of data, several relevant quantities such as the variation of the fluorescence intensity, the photoluminescence (PL) decay and the ACF of the intensity can be extracted.

Post-selection methods can also be carried out. As an example, a time-gated technique was developed to unambiguously distinguish the contribution of clustering and multiexcitonic emis-

sion when a peak at zero delay is observed in antibunching experiments under pulsed excitation [8]. With this full-optical method, it is possible to determine if only one emitter or a cluster is observed. Beyond the scope of the investigation of the time statistics of the photons emitted by a single emitter, post-processing of the stream of photons is widely used in experiments such as entanglement demonstration between a single electron spin and a photon [9, 10, 11].

The PL decay or the ACF for a chosen level of fluorescence intensity corresponding to a given state can also be measured [12]. Such an approach has been applied with success to colloidal quantum dots known to switch between a neutral and an ionized state with different emission intensities (the fluorescence intensity of the ionized state is lower because the trion can recombine through an Auger process [12, 13]). Recently, many authors reported the coupling of colloidal quantum dots to plasmonic structures which enhances the radiative recombinations [14, 15, 16, 17, 18, 19]. Due to the drastic reduction of Auger recombinations, the radiative quantum efficiency of the ionized and neutral states become very close and cannot be distinguished through their intensity [19].

In this paper, we describe a new time-gated technique. Under low excitation power, when a single emitter switches between two emitting states with the same fluorescence intensity but different PL decays, our approach enables to characterize independently the coincidence histogram for each state and get their respective amount of antibunching. After describing the method, we apply it to a typical nanosource consisting in a single colloidal quantum dot coupled to a plasmon resonance. For these thick shell CdSe/CdS core-shell nanostructures inserted into a gold nanoshell resonator, the emission intensities of the ionized and neutral states are equal [19]. We show that the amount of antibunching for the charged and neutral states are different and infer the ratio between the QE of the neutral biexciton and the charged one.

2. Time-gated post-selection

We consider an emitter switching between two states such as a charged and a neutral states for a colloidal quantum dot. We suppose a pulsed laser operation and a low pumping. Fluorescence intensity then corresponds to the recombination of the trion (X^*) and monoexciton (X) that are considered as having the same QE. The charged and neutral states fluorescence intensities are then equal. The calculation of the ACF $g^{(2)}(\tau)$ only involves the photons emitted by the neutral and charged monoexcitons and biexcitons (higher order excitons can be neglected under low excitation). Fundamentally, the post-selection approach is based on the fact that, even if X and X^* exhibit the same QE, the lifetime τ of X is always greater than the lifetime τ^* of X^* because of the number of charge carriers in each excitonic state [12, 19, 20]. Taking into account this general property, the technique consists in selecting the pairs of photons for which the *second* photon is detected for a recombination occurring after a delay longer than D (procedure 1, see Fig. 1) or shorter than D^* (procedure 2, see Fig. 2). The contribution of the ionized state to the coincidences histogram decreases especially as D grows longer whereas it dominates for short values of D^*.

Let us first consider that the emitter remains in a given state (the neutral state for example). With the Hanbury-Brown and Twiss setup, it can be shown that the area of the peak at zero delay is proportional to $Q(1)Q(2)P(2)/2$ where $Q(n)$ is the quantum efficiency of the state with n electron-hole pairs and $P(n)$ the probability to generate this state [6] (in the HBT setup, coincidences are recorded only if the two photons are detected by different photodiodes which explains the factor 1/2). For the lateral peaks, the area is proportional to $[Q(1)P(1)]^2/4$ (the factor 1/4 also comes from the HBT setup). When operating under low excitation and out of any resonance, $P(n)$ follows a poissonian statistics and $P(2) = P(1)^2/2$ [12]. The ratio between the two areas then provides the ratio between the quantum efficiency $Q(2)$ of the biexciton and the quantum efficiency $Q(1)$ of the monoexciton.

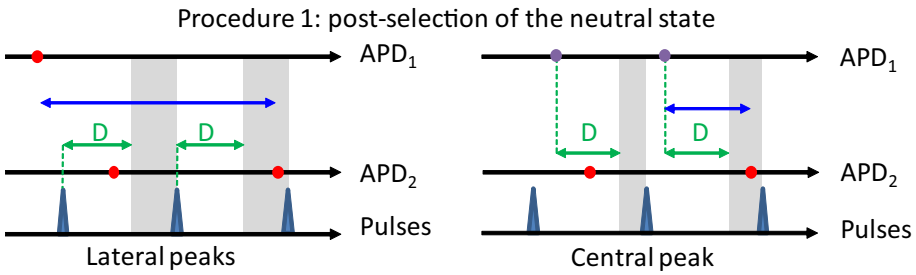

Fig. 1. Schematic representation of the first post-selection procedure that enhances the contribution of the neutral state. The cases of the lateral and central peaks are detailed. The histograms of coincidences are calculated by keeping only the photons arriving within the time-gated region (gray zone). The starting point of this region is defined by D. The double blue arrows indicate the delays selected for the calculation of the coincidences counts. Red/purple dots correspond to detection events on the detectors. Purple (respectively red) dots depict the radiative recombination of a neutral or a charged biexciton (respectively exciton or trion). When a biexcitonic cascade is detected (central peak), it has to be noted that the time-gated region is defined by taking the time detection of the biexciton as reference and not the laser pulse event (see dashed lines).

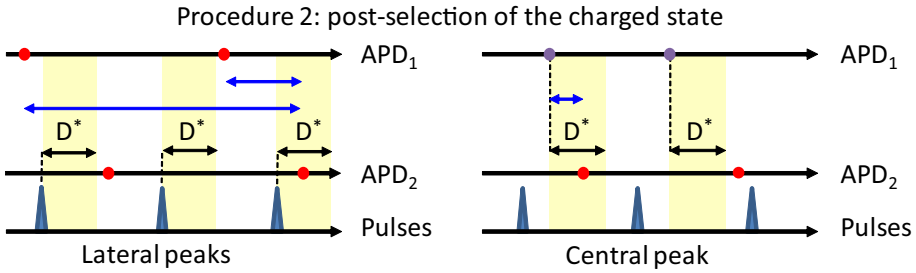

Fig. 2. Schematic representation of the second post-selection procedure that enhances the contribution of the ionized state. The cases of the lateral and central peaks are detailed. The histograms of coincidences are calculated by keeping only the photons arriving within the time-gated region (yellow zone). The duration of this region is defined by D^*. The double blue arrows indicate the delays selected for the calculation of the coincidences counts. Red/purple dots correspond to detection events on the detectors. Purple (respectively red) dots depict the radiative recombination of a neutral or a charged biexciton (respectively exciton or trion). When a biexcitonic cascade is detected (central peak), it has to be noted that the time-gated region is defined by taking the time detection of the biexciton as reference and not the laser pulse event (see dashed lines).

To introduce the procedure 1 of the time-gated post-selection technique, we consider that the emitter is in a fixed state. For a lateral peak of the ACF, the coincidence counts correspond to photons generated by exciton recombinations (see thumbnail image of [6]). We select the photon pairs for which the *second* photon is detected for a delay greater than D after the laser pulse excitation (see Fig. 1, left side). The number of counts is then proportional to $[P(1)Q(1)]^2/4 \times \exp(-D/\tau)$. Indeed, only the second photon of the pair is filtered and the number of photons corresponding to monoexciton recombinations occurring after a delay D is multiplied by a factor $\exp(-D/\tau)$ when compared to the total number of monoexciton recombinations. For the central peak, we have to take into account that the delay between the laser pulse and the second photon is not directly linked to the radiative lifetime τ. Indeed a biexci-

tonic emission precedes the monoexcitonic emission. The radiative lifetime τ then corresponds to the monoexponential decay of the histogram of the delays between the photons generated by the biexciton and monoexciton recombinations. In this case, the post-selection has to be driven by only keeping the coincidence events for which the delay between the two photons is greater than D (see Fig. 1, right side). The area of the peak for delays around zero is then proportional to $Q(1)Q(2)P(2)/2 \times \exp(-D/\tau)$. The crucial point is that the ratio between the peak areas remains unchanged and once again provides the amount of antibunching and the quantum efficiency of the biexciton normalized to the quantum efficiency of the monoexciton.

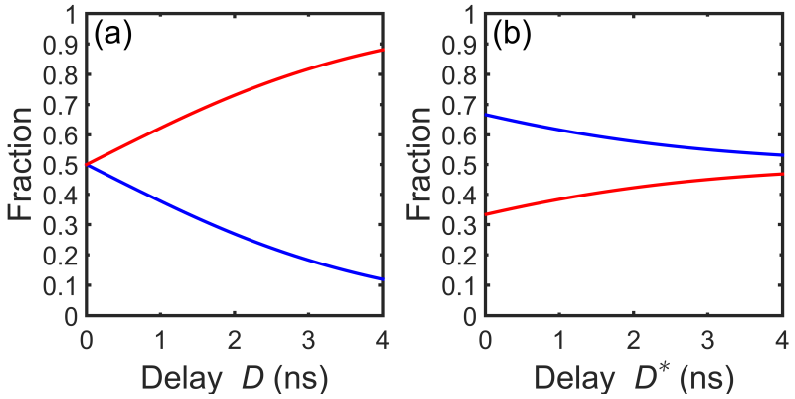

Fig. 3. (a) Fraction of photons corresponding to monoexcitonic (red) and trion (blue) recombination as a function of D. (b) The same as a function of D^*. For the two figures, the emitter spends the same time in the ionized and neutral states and $\tau^* = 1$ ns and $\tau = 2$ ns.

If the emitter switches between a neutral and an ionized state, the fraction of photons corresponding to a radiative trion or a monoexciton recombination can be easily evaluated as a function of the fraction of time spent in each state, the trion and monoexcitonic lifetimes and the delay D. Fig. 3(a) shows the results obtained for an emitter spending the same time in each state with $\tau^* = 1$ ns and $\tau = 2$ ns (values close to the experimental ones discussed in section 3). As seen in Fig. 3(a), when the delay D is 4 times longer than the trion lifetime, the contribution of its radiative recombination can be neglected. In this case, the histogram of the coincidences calculated with the selected pairs of photons will correspond to photons detected only during the neutral state and will provide the ratio between the quantum efficiencies of the neutral biexciton and exciton (this result is valid if the probability of neutral/charged states switching during the time range at which the coincidence histogram is calculated -1 μs in the following- remains negligible).

A time gated analogous approach can also be applied to get insight into the ionized state (procedure 2). One can indeed consider the coincidence events when the second photon is detected at a delay shorter than a given delay D^* (see Fig. 2). In the previous formulas, the term $\exp(-D/\tau)$ is replaced by $[1-\exp(-D^*/\tau^*)]$. However, the situation is less favorable than in the case of monoexciton filtering (see Fig. 3(b)). Since most of the photons corresponding to the monoexciton and trion recombinations are detected at short delays, the contribution of the neutral state cannot be completely suppressed (see Fig. 3(b)).

From a technical point of view, in contrast with many other time-gated techniques, the condition used to select the photon pairs is applied only to the second photon and not to both. Moreover, the delays plotted in the autocorrelation functions are selected considering a gating region defined from the emission of the first photon for the same shot and from the laser pulse

for the other ones.

3. Results and discussion

The two procedures are now applied to thick-shell CdSe/CdS quantum dots encapsulated in a silica shell coated with a gold shell. These hybrid nanostructures were synthesized recently [19] and are referred as golden quantum dots (GQDs) in the following. The coupling between the quantum dot and the plasmonic resonator results in strongly accelerated emission processes that lead to the suppression of Auger recombination of the trion. The QE of the trion and monoexciton are thus equal ($\sim$ 30 % due to metallic losses) and the residual flickering of the thick-shell CdSe/CdS GQD is completely suppressed. Particularly resistant to high power excitation, their emission is perfectly stable.

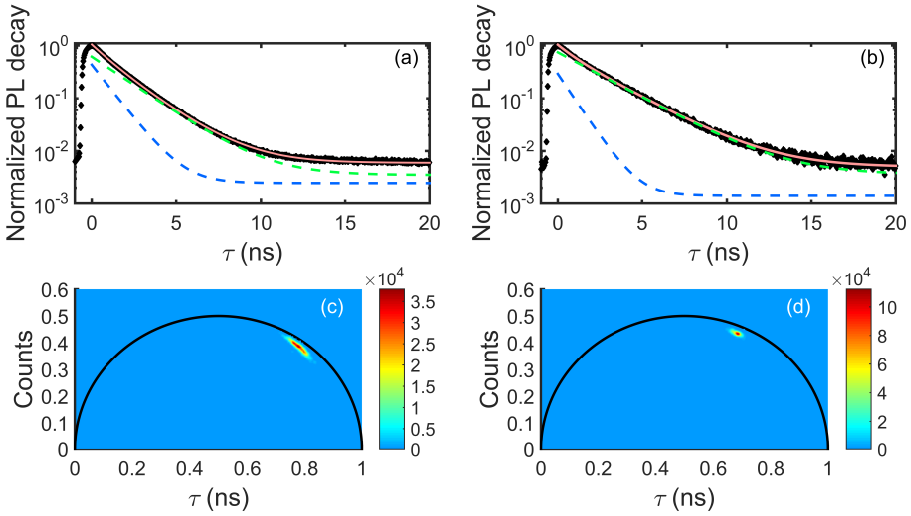

Fig. 4. (a) PL decay of GQD_1. The fit (red line) corresponds to the sum of 2 exponentials decay with a lifetime of 1.1 ns (blue dashed line) and 2 ns (green dashed line) and with a respective amplitude of 0.41 and 0.59. (b) PL decay of GQD_2.The fit (red line) corresponds to the sum of 2 exponentials decay with a lifetime of 0.9 ns (blue dashed line) and 2.5 ns (green dashed line) and with a respective amplitude of 0.28 and 0.72. (c) Polar representation of the fluorescence lifetime of GQD_1. (d) Polar representation of the fluorescence lifetime of GQD_2.

In the following, we consider two GQDs noted GQD_1 and GQD_2. Before applying the two post-selection procedures, we confirm that the emission comes from two different states of the emitter by investigating their PL decay. First, they are well fitted by the sum of two exponential decays from which we deduce the lifetime of each state (Figs. 4(a) and 4(b)). This basic approach can be refined following the procedure described in [21]. After splitting the overall record into intervals of a 1 s duration, we calculate the cosine and sine transforms of the PL decay for each interval that provides the (u,v) coordinates in a polar representation. When a single exponential PL decay is detected, the point is located on a semi-circle. Long lifetimes are on the left of the diagram while short ones are on the right. Multi-exponential decays correspond to points inside the semi-circle. In Figs. 4(c) and 4(d), the results obtained for the two GQDs are plotted by taking into account the number of photons for each point in the diagram through the color bar. For both GQDs, all the points are inside the semi-circle confirming the contribution of two states. For GQD_2, the points are gathered into a very small spot showing

that the lifetimes of the neutral and ionized states as well as the fraction of time spent by the GQD in each state during 1 s are constant. For GQD_1, the linear shape defined by all the points around a central spot can be explained by small variations of the time spent by the GQD in each state during 1 s.

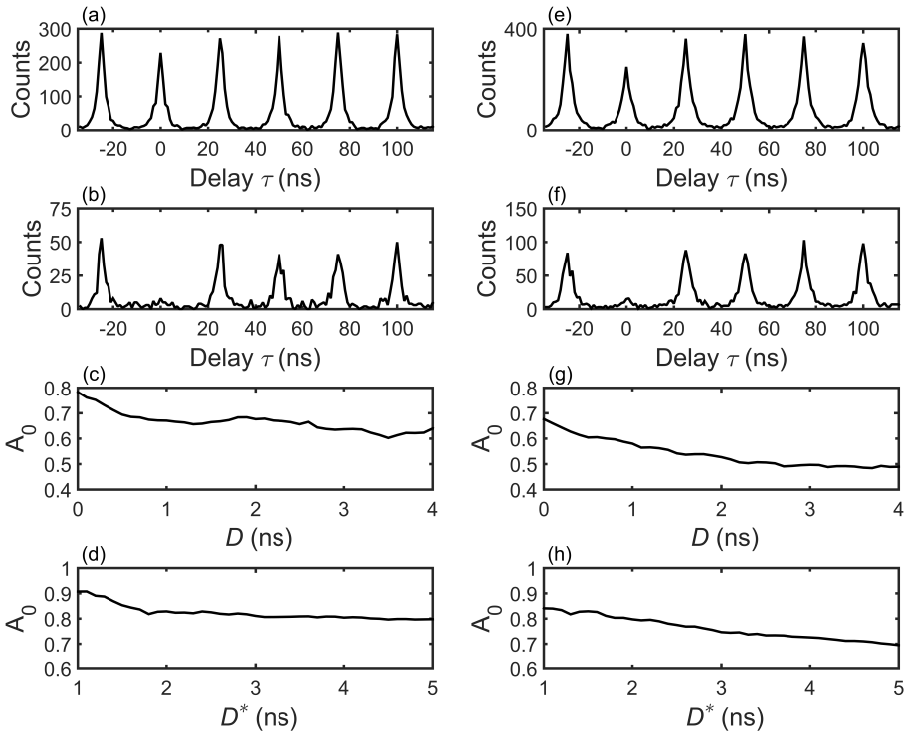

Fig. 5. (a) Overall coincidences counts (GQD_1). (b) Coincidence counts corresponding to photons that have been *both* recorded with a delay greater than 1 ns with respect to the pulse laser (GQD_1, method described in [8]). (c) Area of the central peak normalized to the area of the lateral peaks as a function of D (GQD_1). (d) Area of the central peak normalized to the area of the lateral peaks as a function of D^* (GQD_1). (e), (f), (g) and (h): the same for GQD_2.

The normalized histogram of the delays between photons for the overall record is now plotted for the two GQDs (Figs. 5(a) and 5(e)). A small antibunching is observed for each GQD (20 % for GQD_1 and 30 % for GQD_2). However GQDs are known to form aggregates. In order to prove that we are detecting the fluorescence of a single nanoemitter, we applied the post-selection method proposed by Mangum *et al.* [8] and calculated the histogram of the delays between the photons that are *both* detected for delays greater than 1 ns after the laser pulse. The nearly perfect antibunching (Figs. 5(b) and 5(f)) then observed demonstrates that GQD_1 and GQD_2 correspond to single core-shell nanostructures.

Figs. 5(c), 5(d), 5(g) and 5(h) display the results obtained for the two GQDs by the time-gated procedures. The area of the peak at zero delay normalized to the area of the lateral peaks (noted A_0) versus the time D or D^* are represented. As expected, when increasing D (Figs. 5(c) and 5(g)), A_0 decreases from the value found when the histogram of the coincidences is calculated

with the overall record (0.8 for GQD_1 and 0.7 for GQD_2). It also reaches an asympotical value which means that the application of the procedure 1 permits the suppression of the contribution of the ionized state (see Fig. 3(a)). Moreover, this asymptotic value of A_0 is equal to the QE of the neutral biexciton normalized to the monoexciton one (0.65 for GQD_1 and 0.5 for GQD_2).

The variations of A_0 with D^* (Figs. 5(d) and 5(h)) show the results obtained with the procedure 2 and can be understood as follows. At high values of D^*, A_0 is equal to 0.8 for GQD_1 and 0.7 for GQD_2 since the post-selection has no effect and the contributions of the neutral and ionized states are mixed. When D^* tends to 1 ns, the ionized state dominates. A_0 is close to 0.9 (0.9 for GQD_1 and 0.85 for GQD_2), showing that the QE of the charged biexciton is very close to the trion one in these two GQDs. For these two GQDs, the QE of the neutral biexciton (0.65 and 0.5) is then about 30 % lower than the charged biexciton one (0.9 and 0.85). The results obtained by the two time-gated procedures then reveal the strong difference in the QE of the charged and neutral biexcitons.

4. Conclusion

In conclusion, we presented in detail two original post-selection procedures that can provide the antibunching of the ionized and neutral states of a GQD although they exhibit the same fluorescence intensity. Concerning the photo-physics properties of the emitter, the main result is that the charged and neutral biexcitons do not exhibit the same QE. From a more general point of view, this approach could be applied to other hybrid nanoemitters associating a colloidal quantum dot and a plasmonic nanostructure that have been recently developed.

5. Methods

5.1. Colloidal quantum dots with a nanoshell resonator

The synthesize process of GQDs is described in detail in [19]. Colloidal CdSe/Cs QDs (15 nm radius) are encapsulated in a silica shell ($\sim$ 35 nm) through a water in oil micro emulsion process. The gold shell ($\sim$ 20 nm) is then grown by a two-stage method developed by Halas et al. [22]. The lifetime is typically 12 ns for the monoexcitonic state and 6 ns for the trion. However, for a few GQDs, shorter lifetimes can be observed. We selected such GQDs since a high repetition rate of the pulse laser diode (40 MHz) can be used resulting in a reduction of the data acquisition time.

5.2. Experimental setup

The GQDs were deposited on a glass cover slip and observed at the single molecule level using a standard confocal microscope (Olympus, IX 71) with a 1.4 numerical aperture objective. Optical excitation (λ = 405 nm, repetition rate = 40 MHz, pulsed duration $\sim$ 100 ps) is provided by a pulsed laser diode (Picoquant, LDH P-C-405). The fluorescence is detected though a standard Hanbury-Brown and Twiss setup. The two photodiodes (Picoquant, PDM Series, 50 ps time resolution) are connected to a data acquisition module (Picoquant, PicoHarp 300) operating in the Time-Tagged Time-Resolved mode. Each photodetection event is recorded with an accuracy of 32 ps during the whole experiment.

Acknowledgments

This work has been supported by the Région Ile-de-France in the framework of the DIM "des atomes froids aux nanosciences", the Institut Universitaire de France and by Agence Nationale de la Recherche (Grants No. QDOTICS ANR-12-BS10-0008) for fundings.